

Universal Features of Chiral Symmetry Breaking in Large- N QCD

**Claudio Bonanno,^a Margarita García Pérez,^a Antonio González-Arroyo,^{a,b}
Ken-Ichi Ishikawa,^{c,d} Masanori Okawa,^d Dario Panfalone^e**

^a*Instituto de Física Teórica UAM-CSIC, Calle Nicolás Cabrera 13-15,
Universidad Autónoma de Madrid, Cantoblanco, E-28049 Madrid, Spain*

^b*Departamento de Física Teórica, Universidad Autónoma de Madrid,
Módulo 15, Cantoblanco, E-28049 Madrid, Spain*

^c*Core of Research for the Energetic Universe,
Graduate School of Advanced Science and Engineering,
Hiroshima University, Higashi-Hiroshima, Hiroshima 739-8526, Japan*

^d*Graduate School of Advanced Science and Engineering, Hiroshima University,
Higashi-Hiroshima, Hiroshima 739-8526, Japan*

^e*Department of Physics, University of Turin & INFN, Turin,
Via Pietro Giuria 1, I-10125 Turin, Italy*

E-mail: claudio.bonanno@csic.es, margarita.garcia@csic.es,
antonio.gonzalez-arroyo@uam.es,
ishikawa@theo.phys.sci.hiroshima-u.ac.jp, okawa@hiroshima-u.ac.jp,
dario.panfalone@unito.it

ABSTRACT: We investigate the universal features of chiral symmetry breaking in large- N QCD by comparing non-perturbative determinations of the low-lying Dirac spectrum with chiral Random Matrix Theory (RMT) predictions. Our numerical Monte Carlo calculations are based on a chiral lattice discretization of the Dirac operator, and exploit twisted volume reduction to reach N as large as 841. Matching lattice data with RMT analytic results, we are able to extract the large- N chiral condensate, which is compared with a recent determination obtained with non-chiral Wilson quarks from twisted volume-reduced models.

KEYWORDS: Lattice QCD, $1/N$ Expansion, Chiral Symmetry, Vacuum Structure and Confinement

Contents

1	Introduction	1
2	Random Matrix Theory predictions	3
3	Numerical setup	4
3.1	Lattice action	4
3.2	Lattice chiral Dirac operator	6
4	Numerical results	8
4.1	Checking the chiral properties of the lattice Dirac operator	8
4.2	Scale-invariant RMT predictions	10
4.3	Parameter-dependent RMT predictions	13
4.4	Renormalization of the overlap condensate and comparison with Wilson quarks	16
5	Conclusions	20
A	The spectrum of the free overlap operator	21

1 Introduction

Spontaneous chiral symmetry breaking is a distinctive feature of QCD which has fundamental phenomenological implications for strong interactions, and tight connections with other prominent non-perturbative properties of the theory, such as θ -dependence and confinement. Due to this crucial role, it has been the subject of a large number of studies in the last decades, aiming at improving our understanding of its microscopic origin and of its universal traits.

In this respect, a staple result is provided by the Banks–Casher relation [1]: the realization of chiral symmetry in QCD puts strong constraints on the properties of the low-lying Dirac spectrum. Building on this fundamental finding, it has been argued [2–6] that the eigenvalues of the Dirac operator follow the same universal probability distributions as those of an ensemble of random matrices, where the whole dependence on the microscopic details of the full theory is encoded in a single parameter, identified with the chiral condensate $\Sigma = -\langle\bar{\psi}\psi\rangle$. In the fundamental representation and when N , the number of colors, is larger than 2, the universality class is described by the so-called chiral unitary Random Matrix Theory (RMT). By now, non-perturbative lattice calculations have clearly established this correspondence in QCD from first-principles, both in the chirally-broken phase [7–16] and in the chirally-restored phase sufficiently above the Anderson mobility edge [17–21], by comparing numerical results for the Dirac spectrum with analytic RMT predictions (see also Refs. [22–25] for reviews and further references).

Apart from standard QCD, chiral symmetry breaking plays a fundamental theoretical and phenomenological role also in other QCD-like gauge theories, such as large- N QCD in the 't Hooft limit, obtained when the number of colors N is taken to infinity $N \rightarrow \infty$ at a fixed 't Hooft coupling $\lambda = g^2 N$ and for a fixed number of quark flavors N_f (i.e., $N_f/N \rightarrow 0$). For this reason, in the last two decades chiral symmetry breaking has been extensively studied in this regime on the lattice. However, most of these studies addressed the determination of the chiral condensate either through the Banks–Casher relation, or through the quark mass dependence of the pion mass [26–33], while the investigation of the realization of the universal chiral RMT behavior of the large- N Dirac spectrum has only been addressed in a few seminal papers [34, 35] (see also [36]). The goal of the present paper is to fill this gap and address the universal features of chiral symmetry breaking in large- N QCD via state-of-the-art lattice calculations. To do so, we will consider the Twisted Eguchi–Kawai (TEK) model [37–39].

The TEK model is an effective framework to study lattice gauge theories in the large- N limit by exploiting a fundamental property of large- N gauge theories: the so-called large- N volume reduction [37–48]. In their pioneering paper, Eguchi and Kawai [40] showed that, in the large- N limit, the Yang–Mills lattice theory enjoys a dynamical equivalence between space-time and color degrees of freedom, leading the model to become insensitive to finite-volume effects when $N \rightarrow \infty$. Taking this idea to the extreme, it allows to study large- N gauge theories in the thermodynamic limit even on a volume-reduced 1-site lattice [32, 49–71]. This has the advantage of dramatically reducing the computational burden related to the space-time degrees of freedom, and allows to reach very large values of $N \sim \mathcal{O}(10^2 - 10^3)$ in feasible simulations. Thus, unlike standard approaches to study large- N gauge theories—where the $N = \infty$ limit is typically approached from $N \lesssim 10$ values via extrapolation [28–31, 72–98]—the TEK model practically allows to work directly at $N = \infty$. Large- N volume reduction works provided that center symmetry is unbroken. Spontaneous center symmetry breaking that would occur when reducing the lattice size due to the well-known deconfinement transition [73, 99–109] is avoided in the TEK approach by imposing twisted boundary conditions on the gauge fields in all directions, hence the name of the model.¹ The TEK approach has been extensively used in the last decade, and has allowed to achieve significant progress in the study of several large- N gauge theories, such as large- N QCD [32, 33, 57, 61, 64, 67, 68], large- N SUSY Yang–Mills [69–71], and large- N adjoint QCD [58, 62, 110].

In order to compare RMT predictions with our large- N non-perturbative determinations of the low-lying Dirac eigenvalues, it is of the utmost importance to preserve chiral symmetry even at finite lattice spacing. It is thus imperative to use a lattice formulation of the Dirac operator that satisfies the Ginsparg–Wilson relation [111]. For this reason, we implemented an overlap discretization [112–114] of chiral quarks within our TEK model via the so-called “truncated overlap” approach [115–120]. This approach is presented here for the first time, as previous TEK studies have all employed non-chiral Wilson fermions.

¹This is not the only strategy that has been applied to enforce center symmetry on a small box and achieve large- N volume independence see, e.g., Refs. [41, 45–47].

Our study of the universal traits of the Dirac spectrum will be articulated in two main parts. First, we will compare our results with scale-invariant RMT predictions in order to establish the universal behavior of Dirac eigenvalues in a parameter-agnostic fashion. Then, we will match our results to parameter-dependent RMT analytic results in order to extract the large- N quark condensate $\Sigma/N \sim \mathcal{O}(N^0)$. This will be important for two reasons: first, to verify that different lattice–RMT matching prescriptions lead to the same value of the condensate, and second, to see how this chiral determination of Σ/N compares with the latest TEK one obtained in [33] with non-chiral Wilson quarks.

This paper is organized as follows: in Sec. 2 we provide a compact summary of a few RMT predictions that we aim at checking; in Sec. 3 we discuss our lattice setup, focusing in particular on our TEK implementation of the chiral lattice Dirac operator; in Sec. 4 we discuss our numerical results, focusing on the comparison of lattice data with RMT predictions and on the extraction of the chiral condensate; finally, in Sec. 5 we draw our conclusions and discuss future outlooks of this study.

2 Random Matrix Theory predictions

The relevant universality class to describe large- N QCD is the chiral unitary RMT. Within this effective model, it is possible to derive analytic predictions for the probability distributions $p_k(z_k)$ of the k^{th} eigenvalue z_k of the random matrix ensemble for any fixed topological sector Q [121] (in this discussion the spectrum is assumed to be ordered increasingly, and any degeneracy in the spectrum is assumed to be factored out). As an example, in the $Q = 0$ sector, the distributions of the two lowest eigenvalues z_1 and z_2 and of their ratio $r = z_1/z_2$ are given by [34, 121]:

$$p_1(z_1) = \frac{1}{2} z_1 e^{-\frac{z_1^2}{4}}, \quad (2.1)$$

$$p_2(z_2) = \frac{1}{4} e^{-\frac{z_2^2}{4}} z_2 \int_0^{z_2} du u [I_2(u)^2 - I_1(u)I_3(u)], \quad (2.2)$$

$$p(r) = \frac{1}{4} \frac{r}{(1-r^2)^2} \int_0^\infty du e^{-\frac{u^2}{4(1-r^2)}} u^3 [I_2(u)^2 - I_1(u)I_3(u)], \quad (2.3)$$

with $I_n(x)$ the n^{th} modified Bessel function of the first kind,

$$I_n(x) = \sum_{m=0}^{\infty} \frac{1}{(m+n)! m!} \left(\frac{x}{2}\right)^{2m+n} = \int_0^{2\pi} \frac{d\theta}{2\pi} e^{i\theta n} e^{x \cos(\theta)}. \quad (2.4)$$

In the thermodynamic limit $V \rightarrow \infty$, one expects the following identification to hold, topological sector by topological sector, for the eigenvalues of the massless Dirac operator:

$$z_k = \Sigma V \lambda_k, \quad \not{D} v_{\lambda_k} = i \lambda_k v_{\lambda_k}, \quad \lambda_k \in \mathbb{R}. \quad (2.5)$$

Thus, for asymptotically large volumes, Eq. (2.5) is expected to bridge the RMT eigenvalues z_k and the corresponding Dirac eigenvalues λ_k for all k via a single parameter, the quark condensate Σ . Since on the lattice one typically computes the spectrum of the massless

chiral lattice Dirac operator in a finite volume [10–12, 34, 35], one expects to see deviations from chiral RMT predictions, which should become smaller and smaller and occur for higher and higher k as $V \rightarrow \infty$. Such deviations typically manifest in the fact that, assuming Eq. (2.5), different choices of k lead to different results for Σ .

For this reason, our check of the universal features of the large- N Dirac spectrum will be subdivided into two steps. First, we will monitor deviations of lattice Dirac eigenvalues with respect to RMT predictions in a parameter-free, scale-invariant way by computing the deviation from 1 of the following ratios as a function of the volume:

$$R_{k_1, k_2} \equiv \frac{\langle \lambda_{k_1} \rangle}{\langle \lambda_{k_2} \rangle} \times \left(\frac{\langle z_{k_1} \rangle_{\text{RMT}}}{\langle z_{k_2} \rangle_{\text{RMT}}} \right)^{-1}. \quad (2.6)$$

Here $\langle \mathcal{O} \rangle$ and $\langle \mathcal{O} \rangle_{\text{RMT}}$ denote respectively the expectation values taken in the full theory and in the RMT effective model. Given that in these eigenvalue ratios the factor of ΣV drops and no free parameter can be adjusted, this comparison constitutes a very strong test of the universal traits of the spectrum.

Then, once the correct volume regime has been established, we will move to parameter-dependent RMT predictions, and we will test them by matching lattice data and analytic results to extract the quark condensate assuming the relation (2.5). This can be done either by computing the full probability distribution of the first few eigenvalues and fitting it to RMT predictions, such as those in Eqs. (2.1)–(2.3), or by computing the following ratios:

$$\Sigma V = \frac{\langle z_k \rangle_{\text{RMT}}}{\langle \lambda_k \rangle}. \quad (2.7)$$

These two routes should of course lead to compatible estimates. Since all RMT predictions are described by the same single parameter Σ , we will check that different matching prescriptions—i.e., different choices of k —to extract the chiral condensate give compatible result for the condensate when the corresponding λ_k eigenvalues are in the RMT regime. Moreover, we will compare these determinations of Σ with the one found in [33] for non-chiral Wilson quarks.

3 Numerical setup

This section provides an overview of our lattice discretization for the gluon and the quark sectors, with particular emphasis on the adopted chiral formulation of the Dirac operator, which is implemented for the TEK model in this study for the first time.

3.1 Lattice action

In the 't Hooft large- N limit quarks are quenched, i.e., non-dynamical. From the point of view of lattice simulations, this means that we will draw gluonic configurations from the Monte Carlo according to the pure-gauge action, ignoring the fermion determinant. Then, these gluon fields will constitute the background of the chiral lattice Dirac operator (defined in the next section) which will be employed for spectrum computations.

The TEK partition function of the $d = 4$ single-site TEK model describing the gluonic sector reads:

$$Z_{\text{TEK}} \equiv \int [dU] e^{-S_{\text{W}}[U]}, \quad [dU] \equiv \prod_{\mu=1}^d [dU_{\mu}], \quad (3.1)$$

with $[dU]$ the $SU(N)$ invariant Haar measure and

$$S_{\text{W}}[U] = -Nb \sum_{\mu=1}^d \sum_{\nu \neq \mu} z_{\nu\mu} \text{Tr} \left\{ U_{\mu} U_{\nu} U_{\mu}^{\dagger} U_{\nu}^{\dagger} \right\}, \quad (3.2)$$

the TEK Wilson plaquette action. The Monte Carlo algorithm employed for the sampling of this functional integral is described in detail in Ref. [63]. In Eq. (3.2) $b = 1/(Ng^2)$ is the inverse bare 't Hooft coupling, U_{μ} are the $d = 4$ $SU(N)$ gauge link matrices describing lattice gluon fields, and $z_{\nu\mu}$ is the twist factor used to implement twisted boundary conditions. It is chosen to be a N^{th} -root of unity:

$$z_{\nu\mu} = z_{\mu\nu}^* = \exp \left\{ \frac{2\pi i}{N} n_{\nu\mu} \right\}. \quad (3.3)$$

There are several possible choices of the twist factor; here, we will adopt the so-called *symmetric* twist. This means that N is taken to be a perfect square $N = L^2$, and that the integer-valued anti-symmetric twist tensor $n_{\nu\mu}$ is taken to be:

$$n_{\nu\mu} = -n_{\mu\nu} = k(L)L, \quad (\nu > \mu), \quad (3.4)$$

with $k(L)$ a co-prime integer with L . In the end, thus:

$$z_{\nu\mu} = \exp \left\{ 2\pi i \frac{k(L)}{L} \varepsilon_{\nu\mu} \right\}, \quad \varepsilon_{\nu\mu} = -\varepsilon_{\mu\nu}, \quad \varepsilon_{\nu\mu} = 1 \quad (\nu > \mu). \quad (3.5)$$

As explained in Refs. [39, 122, 123], the flux parameter $k(L)$ and its inverse (mod L) $\bar{k}(L)$ have to be scaled with L to keep $|k|/L$ and $|\bar{k}|/L$ bounded from below (by ~ 0.1) in order to avoid center-symmetry breaking [124–127] that would invalidate one of the assumptions behind large- N volume reduction. In addition, it has been shown in perturbation theory that suitable choices of k, \bar{k} help in reducing non-planar finite- N corrections [65, 128].

As explained in the introduction, even if the TEK model is formulated on a reduced 1-point box, this does not mean at all that our fields propagate in a torus of vanishing volume. Indeed, by virtue of large- N volume independence and of the adopted twisted boundary conditions, physical excitations actually propagate on an extended torus with an effective physical size given by:

$$\ell = aL = a\sqrt{N}, \quad (3.6)$$

with $a(b)$ the lattice spacing. This means that in our setup, at fixed coupling b , the thermodynamic limit is achieved when $N \rightarrow \infty$. It is in this limit that we expect RMT predictions to hold.

3.2 Lattice chiral Dirac operator

The non-chiral TEK Wilson discretization of the Dirac operator, first discussed in Ref. [64], is given by the following $N^2 \times N^2$ matrix (where N^2 is the size of the effective volume in lattice units in the TEK approach):

$$D_W(m_W) = 4 + m_W - \frac{1}{2} \sum_{\mu=1}^d \left[(1 + \gamma_\mu) \otimes \mathcal{W}_\mu + (1 - \gamma_\mu) \otimes \mathcal{W}_\mu^\dagger \right], \quad (3.7)$$

$$\mathcal{W}_\mu = U_\mu \otimes \Gamma_\mu^*, \quad \Gamma_\mu \Gamma_\nu = z_{\nu\mu}^* \Gamma_\nu \Gamma_\mu, \quad (3.8)$$

with Γ_μ the twist eaters [129], $SU(N)$ matrices satisfying $\Gamma_\mu \Gamma_\nu = z_{\nu\mu}^* \Gamma_\nu \Gamma_\mu$, with $z_{\nu\mu}$ the same twist factor appearing in (3.3). To derive this expression, one lets quarks live on an extended periodic lattice with periodicity \sqrt{N} (recall that $z_{\nu\mu}^{\sqrt{N}} = 1$), and let them interact with a periodic potential obtained by replicating the 1-site gauge fields \sqrt{N} times. To some extent, this is reminiscent of the Bloch description of electrons in a crystal.

Building on this non-chiral definition, we can now proceed to define a chiral lattice Dirac operator. For this purpose, we have implemented a chiral Dirac operator using the so-called “truncated overlap” formulation [118–120, 130], whose definition will be summarized in the following. The starting point is the 5d Möbius Domain Wall (DW) Dirac operator [131] (here N_5 is the size of the 5th dimension):

$$D_{\text{DW}}(\hat{m}, M, N_5) = D_W(-M)X(\hat{m}, N_5) + Y(\hat{m}, N_5), \quad (3.9)$$

with \hat{m} the bare quark mass in lattice units. The operator $D_W(-M)$ is the TEK Wilson Dirac operator [64] earlier discussed with a negative kernel mass $M = 1 + s$ ($0 \leq s < 1$), and where we have replaced the standard links U_μ with stout smeared [132] links \bar{U}_μ . Instead, the $X(\hat{m}, N_5)$ and $Y(\hat{m}, N_5)$ operators appearing in Eq. (3.9) are matrices acting on the 5th dimension, whose expressions are:

$$X(\hat{m}, N_5) = B + CM_5(\hat{m}) \quad (3.10)$$

$$Y(\hat{m}, N_5) = 1 + M_5(\hat{m}) \quad (3.11)$$

$$M_5^{(s,t)}(\hat{m}) = (P_L \delta_{s+1,t} + P_R \delta_{s-1,t}) - \hat{m} (P_L \delta_{s,N_5} \delta_{1,t} + P_R \delta_{s,1} \delta_{t,N_5}) \quad (3.12)$$

with $P_L = (1 + \gamma_5)/2$, $P_R = (1 - \gamma_5)/2$ the chiral projectors, and with

$$B^{(s,t)} = b_s \delta_{s,t}, \quad (3.13)$$

$$C^{(s,t)} = c_s \delta_{s,t}, \quad (3.14)$$

diagonal matrices in the 5th dimension. The choice of the vectors b_s and c_s will be discussed later in this section. From D_{DW} , the four-dimensional truncated overlap operator \tilde{D} is built via the following projection:

$$\tilde{D}(\hat{m}, M, N_5) = [\mathcal{P} D_{\text{DW}}^{-1}(M, \hat{m} = 1, N_5) D_{\text{DW}}(M, \hat{m}, N_5) \mathcal{P}]_{1,1}, \quad (3.15)$$

with $\mathcal{P} = P_L \delta_{s,t} + P_R (\delta_{s+1,t} + \delta_{s,1} \delta_{t,N_5})$. This yields the following expression for the truncated overlap [118, 119, 130, 131] that we will use in our study:

$$\tilde{D}(\hat{m}, M, N_5) = \frac{1 + \hat{m}}{2} 1 + \frac{1 - \hat{m}}{2} \gamma_5 S(M, N_5). \quad (3.16)$$

In this expression, the function $S(M, N_5)$ is given by:

$$S(M, N_5) = \frac{\prod_{s=1}^{N_5} [1 + \mathcal{H}_W^{(s)}(M)] - \prod_{s=1}^{N_5} [1 - \mathcal{H}_W^{(s)}(M)]}{\prod_{s=1}^{N_5} [1 + \mathcal{H}_W^{(s)}(M)] + \prod_{s=1}^{N_5} [1 - \mathcal{H}_W^{(s)}(M)]}, \quad (3.17)$$

with

$$\mathcal{H}_W^{(s)}(M) = (b_s + c_s) \gamma_5 D_W(-M) [(b_s - c_s) D_W(-M) + 2]^{-1}. \quad (3.18)$$

The choice of the vectors b_s and c_s is arbitrary as long as $S(M, N_5)$ reproduces the sign function of overlap fermions in the limit $N_5 \rightarrow \infty$. Different choices correspond to different lattice formulations, including Shamir-, Boriçi-, and Chiu-type realizations of domain wall fermions [116–118, 133], all agreeing in the continuum limit. In this study we chose $b_s = 1$ and $c_s = 0$, corresponding to the Shamir operator. With this choice, we obtain:

$$S(M, N_5) = \frac{[1 + \mathcal{H}_W(M)]^{N_5} - [1 - \mathcal{H}_W(M)]^{N_5}}{[1 + \mathcal{H}_W(M)]^{N_5} + [1 - \mathcal{H}_W(M)]^{N_5}}, \quad (3.19)$$

with $\mathcal{H}_W(M)$ the (γ_5 -Hermitian) kernel

$$\mathcal{H}_W(M) = \gamma_5 D_W(-M) [2 + D_W(-M)]^{-1}. \quad (3.20)$$

In the limit $N_5 \rightarrow \infty$, when the size of the 5th dimension goes to infinity, we recognize that $S(M, N_5)$ tends to the sign of the kernel $\mathcal{H}_W(M)$:

$$\lim_{a \rightarrow \infty} \frac{(1+x)^a - (1-x)^a}{(1+x)^a + (1-x)^a} = \text{sign}(x). \quad (3.21)$$

Therefore, in the limit $N_5 \rightarrow \infty$, the truncated overlap tends to the actual overlap operator:

$$\lim_{N_5 \rightarrow \infty} \tilde{D}(\hat{m}, M, N_5) = D(\hat{m}, M), \quad (3.22)$$

which takes the form

$$D(\hat{m}, M) = \frac{1 + \hat{m}}{2} 1 + \frac{1 - \hat{m}}{2} V(M) = (1 - \hat{m}) D_0(M) + \hat{m}, \quad (3.23)$$

with $V(M) = \gamma_5 \text{sign}[\mathcal{H}_W(M)]$, and $D_0(M)$ the massless overlap operator,

$$D_0(M) = \frac{1 + V(M)}{2}. \quad (3.24)$$

In order to restore physical units in the lattice operator D and in the lattice mass \hat{m} and connect them to their physical counterparts, one needs to perform the following rescaling:

$$\not{D} = \frac{M(2-M)}{a} D_0(M) \quad (3.25)$$

$$m = \frac{M(2-M)}{a} \hat{m}, \quad (3.26)$$

where m is the *bare* quark mass in physical units. The pre-factor $M(2-M)$, which stems from the choice of the kernel in Eq. (3.20), was worked out analytically by requiring that the spectrum of the massless operator in Eq. (3.25) in the free case was equal to \not{p} in momentum space. More details can be found in the Appendix (see also Ref. [134]). Clearly, the same normalization applies when restoring physical units in the eigenvalues of the massless overlap Dirac operator:

$$D_0(M)u_{\hat{\lambda}} = \hat{\lambda}(M)u_{\hat{\lambda}}, \quad (3.27)$$

$$\hat{\lambda}(M) = \frac{1}{2} \left[1 + e^{i\theta(M)} \right], \quad (3.28)$$

$$\lambda_o = \frac{M(2-M)}{a} \hat{\lambda}(M). \quad (3.29)$$

Apart from this necessary overall rescaling, M is expected to play no other role, and any possible weak M -dependence observed in a physical quantity is just a lattice artifact vanishing in the continuum limit, see, e.g., Ref. [135].

4 Numerical results

This section is devoted to present our non-perturbative lattice results for the low-lying chiral Dirac spectrum, and to discuss the comparison with RMT predictions. As already anticipated, we will conduct such comparison both in a parameter-free and in a parameter-dependent fashion. The latter approach will also allow the extraction of the large- N chiral condensate $\Sigma/N \sim \mathcal{O}(N^0)$, whose value will be compared with the latest large- N TEK determination with non-chiral Wilson quarks [33]. Simulation parameters are summarized in Tab. 1, along with the value of the string tension σ from the TEK model [57], used for scale setting.

4.1 Checking the chiral properties of the lattice Dirac operator

We start our discussion by examining the chiral properties of the truncated overlap operator. Indeed, one should check that the adopted N_5 is large enough to have sufficiently small chirality violations (i.e., a negligible residual mass). These are monitored through the figure of merit:

$$\Delta = \frac{1}{|z|} \left| \left(\{\tilde{D}, \gamma_5\} - 2\tilde{D}\gamma_5\tilde{D} \right) z \right|, \quad (4.1)$$

which quantifies the violation of the Ginsparg–Wilson relation.

b	N	$L = \sqrt{N}$	k	k/L	\bar{k}	\bar{k}/L	$a\sqrt{\sigma}$	n_{conf}
0.355	529	23	7	0.304	10	0.435	0.2410(30)	400
0.360	289	17	5	0.294	7	0.412	0.2058(25)	326
	361	19	7	0.368	11	0.579		189
	529	23	7	0.304	10	0.435		222
	841	29	9	0.310	13	0.448		210

Table 1: Values of the number of colors N , of the effective size $L = \sqrt{N}$, and of the parameters k, \bar{k} [where $\bar{k}k = 1 \pmod{L}$] used in this study. The string tension σ was computed in the TEK model in [57]. Finally, n_{conf} is the number of statistically-independent gauge configurations employed.

The violation parameter Δ was computed stochastically using 3 random \mathbb{Z}_4 -sources z with color and Dirac indices. After a few tests, we concluded that, in order to achieve satisfactory small values of Δ , smaller values of N_5 were sufficient when the gauge links entering the truncated overlap Dirac operator were smeared. As an example, $\Delta \sim 10^{-8}$ was achieved with $N_5 = 60$ and no smearing, while the same result was obtained choosing $N_5 = 24$ and $n_s = 5$ stout-smearing steps (with isotropic stout parameter $\rho = 0.1$ [132]). The latter choice of smearing parameters corresponds to a smearing radius [136]:

$$\frac{R_s}{a} = \sqrt{8\rho n_s} = 2. \quad (4.2)$$

This is equal in magnitude to the choice adopted in other stout-smearing definitions of the lattice Dirac operator employed in recent state-of-the-art lattice QCD simulations. For example, the BMW collaboration recently employed a stout-smearing definition of the staggered Dirac operator with $n_s = 4$ and $\rho = 0.125$ —corresponding to $R_s/a = 2$ —in their recent lattice investigations of the hadronic vacuum polarization contribution to the muon anomalous magnetic moment [137, 138].

The choice of using stout-smearing links was also useful to reduce the computational burden and make $N = 841$ calculations feasible. Indeed, at fixed N , N_5 , and number of computed eigenvalues, we found that spectra calculations involving the stout-smearing operator were ~ 3 times less expensive with respect to the non-smearing case, on top of the ~ 2.5 reduction of N_5 at fixed Δ achieved using stout smearing, which decreases the computational effort by the same factor. Thus, all our results have been obtained for $N_5 = 24$ and stout-smearing gauge links with $n_s = 5$ and $\rho = 0.1$, yielding $\Delta \lesssim 10^{-8}$ for all explored values of N and b .

Another interesting test of the good chiral properties of our truncated overlap Dirac operator is to check that lattice eigenvalues lie on the overlap circle:

$$\hat{\lambda} = \frac{1}{2} + \frac{1}{2}e^{i\theta}, \quad (4.3)$$

with $\hat{\lambda}$ the eigenvalue of the massless overlap operator. In Fig. 1 we plot as an example the first two complex eigenvalues $\hat{\lambda}_1$ and $\hat{\lambda}_2$. Due to γ_5 -hermiticity, eigenvalues come in pairs that have the same real part and opposite imaginary parts. Thanks to this symmetry, we can just limit to plot the upper half of the circle in the complex plane. The plots in Fig. 1

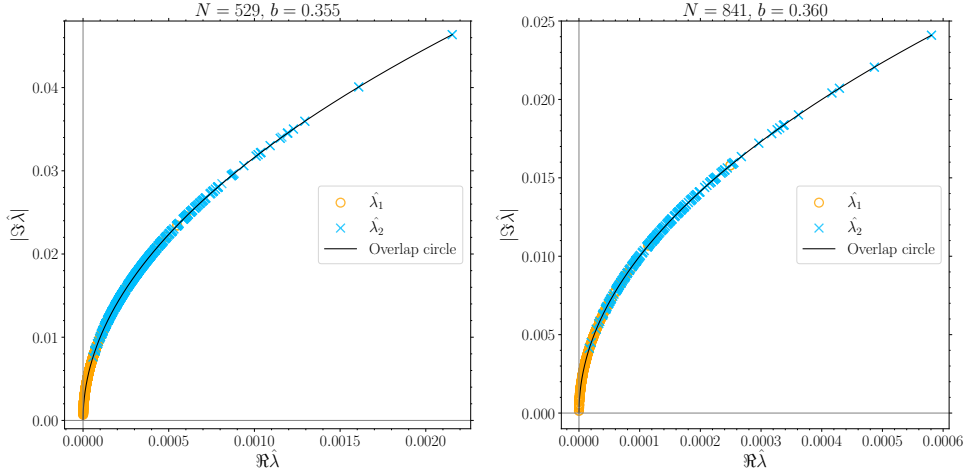


Figure 1: First two complex eigenvalues of the truncated overlap Dirac operator obtained with $M = 1.2$, $N_5 = 24$ and stout-smear gauge links with stout parameters $\rho = 0.1$, $n_s = 5$, corresponding to a smoothing radius of two lattice spacings. The solid black line stands for the expected overlap circle (4.3) in the complex plane. Left panel: $N = 529$, $b = 0.355$. Right panel: $N = 841$, $b = 0.360$.

refer to the cases $N = 529$ at $b = 0.355$ and $N = 841$ at $b = 0.360$, corresponding to similar effective sizes in physical units:

$$b = 0.355, N = 529 \quad \Longrightarrow \quad \ell\sqrt{\sigma} = (a\sqrt{\sigma})\sqrt{N} \simeq 5.54, \quad (4.4)$$

$$b = 0.360, N = 841 \quad \Longrightarrow \quad \ell\sqrt{\sigma} = (a\sqrt{\sigma})\sqrt{N} \simeq 5.97. \quad (4.5)$$

As it can be observed, all eigenvalues of all configurations considered indeed lie on the overlap circle for $N_5 = 24$ and our choice of smearing parameters. It is worth commenting that the eigenvalues displayed in the plot were obtained by choosing the free parameter M appearing in the overlap operator as $M = 1.2$. After checking for the $N = 289$ ensemble that $M = 1.5$ gave perfectly compatible results for the eigenvalue distributions, we kept this choice throughout all calculations.

4.2 Scale-invariant RMT predictions

To test the agreement between our overlap eigenvalues and Random Matrix Theory (RMT), we analyzed the ratios defined in Eq. (2.6), and quantified their deviation from unity. In order to compute the expectation values $\langle \lambda_k \rangle$, we computed the first few low-lying eigenvalues of the massless overlap operator for a few hundred gauge configurations, and we identified the physical Dirac eigenvalue λ with the absolute value of the overlap one λ_o :

$$\lambda \longrightarrow |\lambda_o|, \quad a\lambda_o = M(2 - M)\hat{\lambda}. \quad (4.6)$$

Clearly, we could have also opted for the imaginary part of λ_o as well, being the real part just a lattice artifact that vanishes in the continuum limit. However, we practically observed no numerical difference between $\langle \text{Im}\{\lambda_o\} \rangle$ and $\langle |\lambda_o| \rangle$, as $\text{Re}\{\lambda_o\}$ turned out to be always at least one order of magnitude smaller than $\text{Im}\{\lambda_o\}$ for all computed eigenvalues,

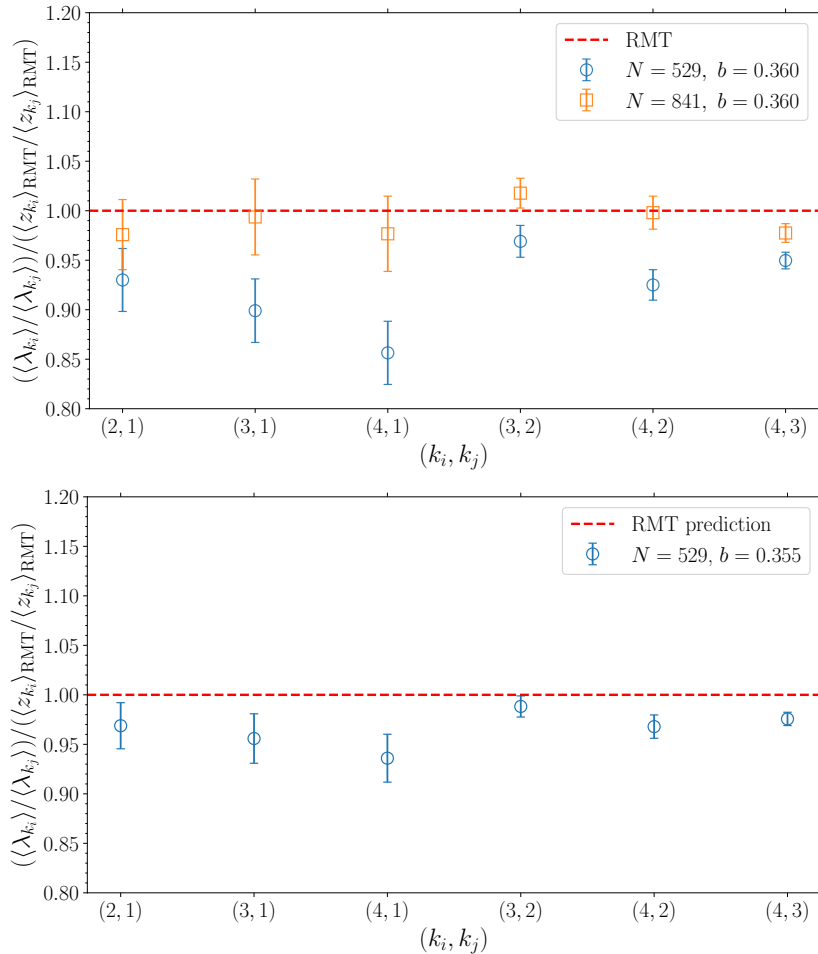


Figure 2: Ratios of expectation values $\langle \lambda_{k_1} \rangle / \langle \lambda_{k_2} \rangle$, obtained considering all combinations with $k_i, k_j \leq 4$, divided by the same quantity computed in the RMT model, $\langle z_{k_1} \rangle_{\text{RMT}} / \langle z_{k_2} \rangle_{\text{RMT}}$. The red dashed line at $y = 1$ represents the agreement between lattice data and RMT predictions. Top and bottom panels refer, respectively, to $b = 0.360$ and $b = 0.355$.

see Fig. 1. Concerning the RMT predictions $\langle z_{k_1} \rangle_{\text{RMT}} / \langle z_{k_2} \rangle_{\text{RMT}}$, the numerical evaluations of the analytic results for these ratios are taken from Tab. VII of Ref. [12]. Finally, concerning the topological sector, we did not find any exact zero-mode in our spectra, thus, we compared our data with RMT predictions in the $Q = 0$ topological sector.

In Fig. 2 we plot the results obtained for $b = 0.355$ and $b = 0.360$, for several choices of k_1 and k_2 . Let us first comment the $b = 0.360$ case, where two values of N are reported. As it can be seen, for $N = 529$, corresponding to $\ell\sqrt{\sigma} \simeq 4.73$, one can clearly observe deviations from RMT predictions, which can become as large as $\sim 15\%$. Smaller values of $N = 289, 361$, not shown in the plot, exhibit even larger deviations. On the other hand, when N is increased to 841, corresponding to the larger size $\ell\sqrt{\sigma} \simeq 5.97$, we observe perfect agreement with RMT predictions within errors in all examined cases, up to $k_1, k_2 = 4$. For the coarser point $b = 0.355$, where $N = 529$ corresponds to $\ell\sqrt{\sigma} = 5.54$ (i.e., an intermediate volume between the two earlier discussed), we observe small deviations of the

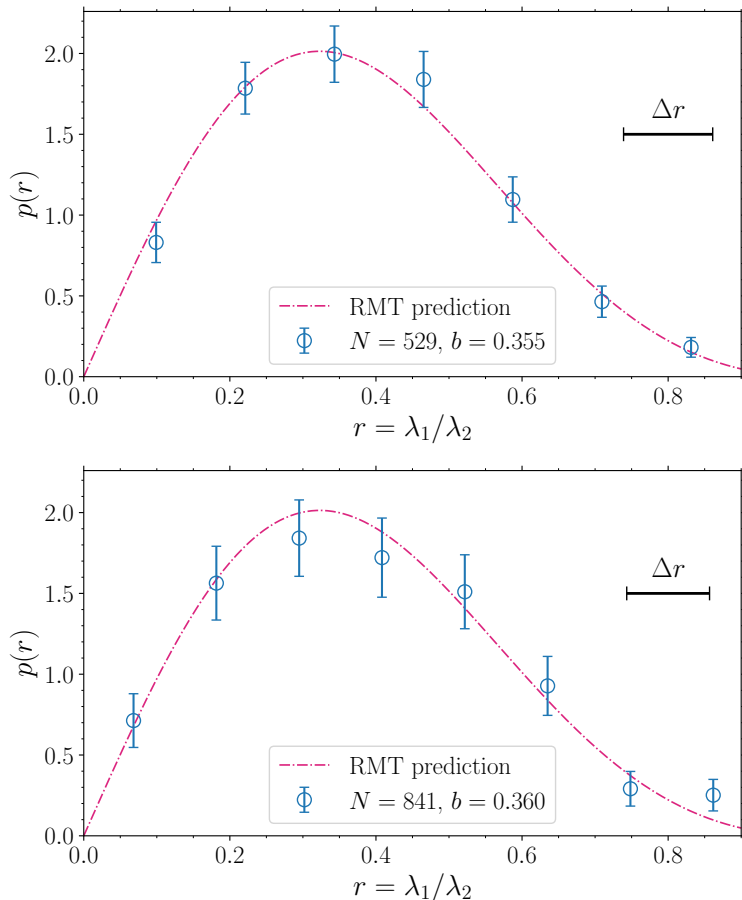


Figure 3: Distribution of the ratio of the first two Dirac eigenvalues, $r = \lambda_1/\lambda_2$. Top panel: $N = 529$, $b = 0.355$. Bottom panel: $N = 841$, $b = 0.360$. The dashed curve represents the parameter-free functional form predicted by RMT for $p(r)$, reported in Eq. (2.3). In all plots we also show the constant bin size Δr used to obtain the displayed distributions.

order of a few percent ($\sim 5\%$ at most). Overall, thus, the collected evidence shows that finite-volume effects play a crucial role in the present analysis, and that the agreement between lattice data and RMT predictions is controlled by the effective size in physical units. As $\ell \rightarrow \infty$, i.e., as $N \rightarrow \infty$ at fixed b , RMT predictions become more and more accurate.

Analogous conclusions can be drawn by comparing the lattice distribution of the ratio of eigenvalues $r = \lambda_1/\lambda_2$ with the parameter-free RMT prediction for $p(r)$ in Eq. (2.3). As it can be seen in Fig. 3, the numerical results for the normalized distribution of r ,

$$p(r) = \frac{\langle \text{number of } \frac{\lambda_1}{\lambda_2} \in [r - \frac{1}{2}\Delta r, r + \frac{1}{2}\Delta r] \rangle}{n_{\text{conf}} \Delta r}, \quad (4.7)$$

obtained for the two largest effective sizes explored — namely, $N = 529$ at $b = 0.355$ and $N = 841$ at $b = 0.360$ — agree very well with expectations. We stress again that the curves shown in Fig. 3 are scale-invariant RMT predictions with no free parameter, and thus there is no fitting procedure involved in the comparison with numerical data.

4.3 Parameter-dependent RMT predictions

Our previous analysis showed that an effective size $\ell\sqrt{\sigma} \gtrsim 5.5$ is sufficient for the first few Dirac eigenvalues to fall into the RMT regime. The goal of this section is to check that their parameter-dependent probability distribution is indeed described by the analytic RMT functional form with the same parameter Σ .

In the large- N TEK case, the relation between RMT and Dirac eigenvalues in (2.5) is modified as:

$$z_k = \lambda_k \frac{\Sigma}{N} V, \quad V = a^4 N^2, \quad (4.8)$$

where we performed the substitution $\Sigma \rightarrow \Sigma/N$, which is the quantity that possesses a finite large- N limit, and where we have used the fact that in the TEK model the lattice size $\ell = aL$ is replaced by the effective torus size $\ell = aL = a\sqrt{N}$. There are two possible ways to extract Σ/N from RMT predictions:

- (1) Performing a best fit of the normalized lattice probability distribution of $a\lambda_k$ to the expected RMT shapes assuming the following relation:

$$z_k = (a\lambda_k)A, \quad A = a^3 \frac{\Sigma}{N} N^2, \quad (4.9)$$

with A the only fit parameter. For example, the normalized RMT probability distribution for the first eigenvalue $x_1 \equiv a\lambda_1$ assuming (4.9) reads:

$$p_1(x_1) = \frac{1}{2} (A^2 x_1) e^{-\frac{1}{4} A^2 x_1^2}. \quad (4.10)$$

This strategy, adopted in [34, 35], does not only allow to extract the condensate, but also constitutes a strong test of the agreement between lattice data and RMT predictions.

- (2) From Eq. (4.8), computing this ratio of expectation values:

$$a^3 \frac{\Sigma}{N} = \frac{\langle z_k \rangle_{\text{RMT}}}{N^2 \langle a\lambda_k \rangle}, \quad (4.11)$$

where

$$\langle z_k \rangle_{\text{RMT}} = \int_0^\infty z_k p_k(z_k) dz_k. \quad (4.12)$$

This strategy (2) has been applied in previous standard QCD studies to extract the condensate from RMT predictions [10–16]. Clearly, it should provide compatible estimates for Σ/N with respect to (1).

For the two largest effective volumes ($N = 529$ for $b = 0.355$ and $N = 841$ for $b = 0.360$), best fits of lattice data for the probability distribution of the first few eigenvalues yield satisfactory reduced chi-squared $\tilde{\chi}^2 \equiv \chi^2/n_{\text{dof}}$, confirming the quality of the RMT description. As an example, we show in Fig. 4 the best fits of the numerical probability

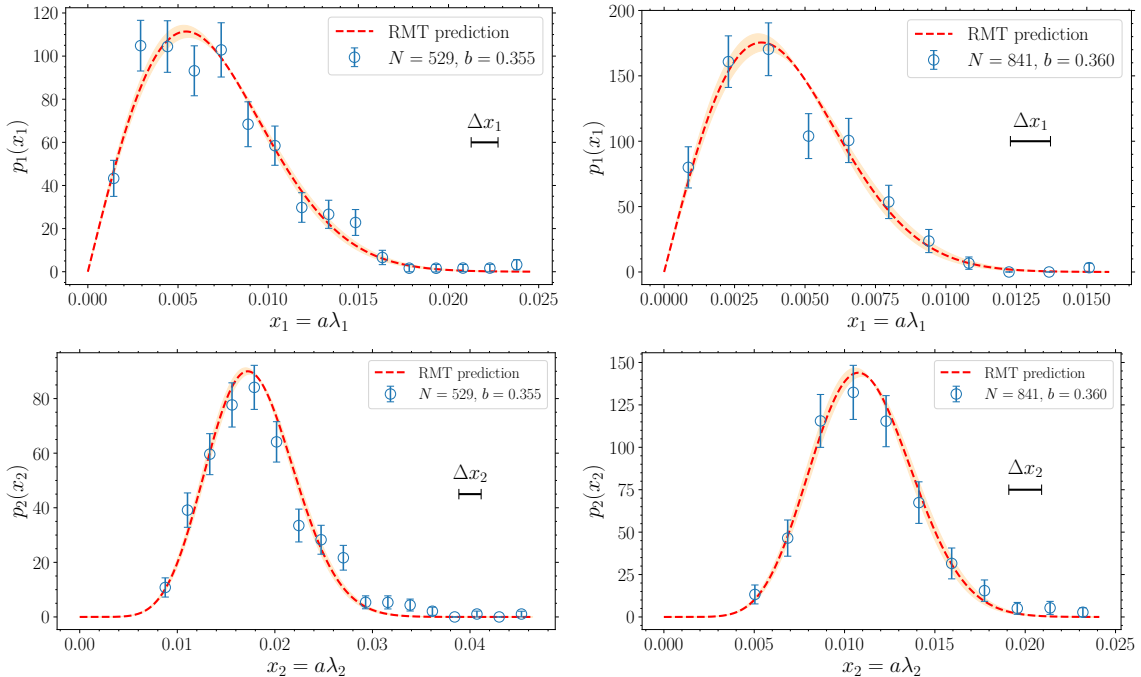


Figure 4: Best fits of the probability distribution of the first (top panels) and the second (bottom panels) eigenvalues according to, respectively Eqs. (2.1) and (2.2). Left panels refer to $N = 529, b = 0.355$, right panels to $N = 841, b = 0.360$. In all plots we also show the constant bin sized Δx_1 and Δx_2 used to obtain the displayed distributions.

	N	b	$\tilde{\chi}^2$	p -value	$10^3 \times a^3 \Sigma / N$ [RMT fit]	$10^3 \times a^3 \Sigma / N$ [Eq. (4.11)]
λ_1	529	0.355	0.99	46%	0.891(22)	0.870(24)
	841	0.360	0.89	52%	0.556(20)	0.561(22)
λ_2	529	0.355	1.90	2%	0.931(12)	0.899(14)
	841	0.360	0.55	86%	0.587(10)	0.575(11)

Table 2: Extraction of the large- N condensate from the first two low-lying eigenvalues, both from the best fit to RMT predictions for their probability distribution and via Eq. (4.11).

distributions of the first two eigenvalues, λ_1 and λ_2 . We report the results for the chiral condensate (i.e., the fit parameter A) extracted from the best fit in Tab. 2, along with the compatible determinations obtained from the ratio of expectation values in Eq. (4.11). As it can be seen, the estimates obtained from λ_1 and λ_2 perfectly agree within errors, in agreement with RMT predictions. On the other hand, when lowering the effective volume, probability distributions start to show deviations from RMT, and the condensates extracted from different choices of λ_k are clearly different from each other, cf. Tab. 3.

b	N	$10^3 \times a^3 \Sigma / N$ [From λ_1]	$10^3 \times a^3 \Sigma / N$ [From λ_2]	$10^3 \times a^3 \Sigma / N$ [From λ_3]	$10^3 \times a^3 \Sigma / N$ [From λ_4]
0.360	289	0.516(15)	0.672(10)	0.7823(69)	0.8940(64)
	361	0.510(22)	0.605(13)	0.6681(96)	0.7550(88)
	529	0.537(21)	0.580(13)	0.598(11)	0.6268(83)
	841	0.561(22)	0.575(11)	0.565(11)	0.5764(81)

Table 3: Bare chiral condensate in lattice units obtained from Eq. (4.11) for several choices of k , and as a function of N .

The differences observed at smaller values of N in the condensates extracted from higher eigenvalues, as discussed in the previous section, can be regarded as finite-volume effects due to not being yet in the regime where RMT provides a reliable description. It is known that RMT is expected to hold in the so-called ϵ -regime of QCD [139], see, e.g., Refs. [22, 140]. Customarily, QCD is studied in the so-called p -regime, obtained taking first the thermodynamic limit $L \rightarrow \infty$ at fixed and finite quark mass and then the chiral limit, so that $m_\pi L \rightarrow \infty$. In the ϵ -regime, instead, $m \rightarrow 0$ and $L \rightarrow \infty$ with $m\Sigma V \lesssim \mathcal{O}(1)$. Since $m\Sigma V = 2(F_\pi m_\pi L^2)^2$, this means that $m_\pi L \rightarrow 0$ while $F_\pi L \rightarrow \infty$. It was shown in Ref. [139] that finite-volume corrections to the thermodynamic limit in the ϵ -regime are power-like, and can be expanded in series of the variable $1/(F_\pi^2 L^2) = 1/(F_\pi^2 \sqrt{V})$. This behavior is very different from the customary exponential suppression of finite-size effects in the p -regime, and is related to the peculiar way of taking the chiral and thermodynamic limits.

We empirically tried to check whether the volume-dependence of our data can be described by polynomials in the variable $x = 1/\sqrt{V}$ or not, with $V = a^2 N^2$ the effective volume. Interestingly, our results for the condensate for $b = 0.360$ as a function of N obtained from the first four low-lying eigenvalues can be all well described by polynomial curves in this variable, extrapolating to compatible values at $x = 0$, and with similar slopes close to zero, see Fig. 5 (left panel). From these fits we can quote the following final result:

$$\frac{a^3 \Sigma}{N} = 0.605(35) \times 10^{-3}. \quad (4.13)$$

where the central value is the average of the four extrapolations, and the quoted error is the maximum semi-dispersion observed among them. The observed behavior of the best fits performed on a k -by- k basis also lead us to try a global best fit of the data, assuming the following functional form:

$$\frac{a^3 \Sigma_k}{N} = B_0 \left(1 + B_1 \frac{x}{\sigma} + B_2^{(k)} \frac{x^2}{\sigma^2} \right), \quad x = \frac{1}{\sqrt{V}} = \frac{1}{a^2 N}, \quad (4.14)$$

where Σ_k is the condensate extracted from λ_k , and where we impose a common large-volume limit B_0 and a common slope B_1 . This functional form describes our data very well, giving $\tilde{\chi}^2 \simeq 0.83$, see also Fig. 5 (right panel). Moreover, it gives a compatible

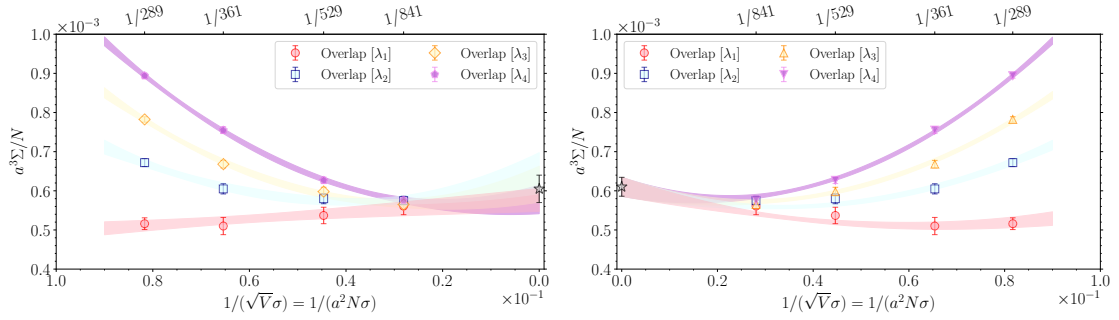


Figure 5: The bare large- N chiral condensate Σ/N in lattice units as a function of $1/\sqrt{V}$. Left panel: shown curves are polynomial fits in $1/\sqrt{V}$ to each individual data set. Right panel: shown curves are the result of a global best fit according to the empirical ansatz in Eq. (4.14) (bottom panel).

thermodynamic limit with respect to the one obtained from the unconstrained fit:

$$\frac{a^3 \Sigma}{N} = 0.610(24) \times 10^{-3}. \quad (4.15)$$

Although both extrapolated results are larger, they are nevertheless compatible within errors with the average of the $N = 841$ results:

$$\frac{a^3 \Sigma}{N} = 0.575(25) \times 10^{-3}. \quad (4.16)$$

where again the error is the sum of a statistical and a systematic one, taking into account the dispersion among the data. In order to be conservative, we will consider the result in Eq. (4.13) as our final overlap determination for $b = 0.360$, as this has the largest error among the results in Eqs. (4.13), (4.15) and (4.16).

Clearly, apart from polynomials in $1/\sqrt{V}$, also other functional forms could equally well describe our data. Thus, to really pinpoint the exact form of finite-size corrections, more theoretical studies would be needed to work out the expected ϵ -regime volume-dependence of QCD low-energy constants in the TEK model. This is left for future studies.

4.4 Renormalization of the overlap condensate and comparison with Wilson quarks

In order to compare our overlap determination of Σ/N with the previous TEK one obtained in Ref. [33] with Wilson fermions, it is necessary to renormalize Σ . The overlap valence quark mass and the overlap chiral condensate renormalize as follows:

$$\Sigma_{\text{R}} = Z_{\text{S}} \Sigma, \quad (4.17)$$

$$m_{\text{R}} = Z_{\text{m}} m = \frac{1}{Z_{\text{S}}} m, \quad (4.18)$$

where $am = M(2-M)\hat{m}$, and where we used the relation $Z_{\text{m}} Z_{\text{S}} = 1$, holding by virtue of the lattice chiral symmetry. These renormalization constants depend on the renormalization scheme s and on the renormalization scale μ . From now on, any presented renormalized

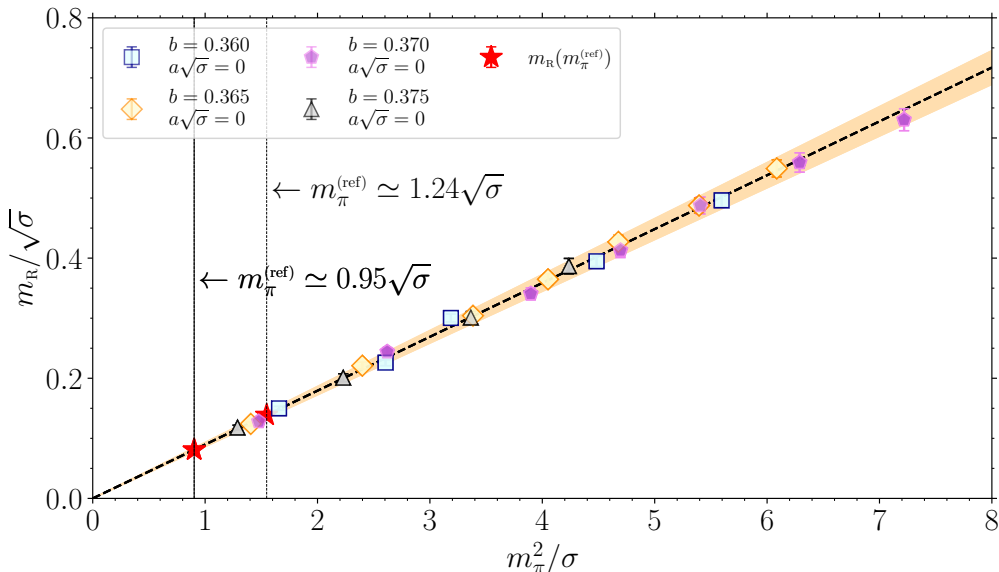


Figure 6: Continuum determination of the renormalized quark mass as a function of the pion mass. Fitted data come from [33] and have been obtained with Wilson fermions.

quantity will be expressed according to the standard choices of renormalization scheme and scale: $s = \overline{\text{MS}}$ and $\mu = 2$ GeV. In this work we assume $\mu = 2$ GeV $\rightarrow \mu/\sqrt{\sigma} = 3.75$ as in the previous large- N studies [31, 33].

In order to compute Z_S , we follow the strategy put forward in Ref. [11]. In this study, the authors obtained Z_S for overlap quarks from the ratio of the bare overlap mass and the continuum renormalized mass matched at equal values of the pion mass, for a certain reference value $m_\pi = m_\pi^{(\text{ref})}$:

$$Z_S = \frac{m \Big|_{m_\pi = m_\pi^{(\text{ref})}}}{m_R \Big|_{m_\pi = m_\pi^{(\text{ref})}}}. \quad (4.19)$$

Following again the lines of Ref. [11], we compute the continuum renormalized quark mass m_R as a function of m_π using Wilson fermion results. Within the TEK model, we computed the Wilson pion mass as a function of the bare Wilson quark mass [33]. Concerning non-perturbative determinations of Z_S needed to renormalize the bare Wilson quark mass, in absence of direct TEK determinations, we relied on the finite- N determinations of [141], suitably extrapolated towards $N = \infty$ and interpolated at our values of the lattice spacing. We refer the reader to Ref. [33] for more details on this point.

First, we computed the renormalized mass in physical units for several values of the hopping parameter κ and of the coupling b (here κ_c is the critical hopping parameter):

$$\frac{1}{\sqrt{\sigma}} m_R(b, \kappa) = \frac{1}{Z_S(b)} \frac{1}{a(b)\sqrt{\sigma}} \left(\frac{1}{2\kappa} - \frac{1}{2\kappa_c(b)} \right). \quad (4.20)$$

Then, we performed the following global best fit as a function of b and κ :

$$\frac{1}{\sqrt{\sigma}} m_R(b, \kappa) = A_1 x_1(b) + A_2 x_2(b, \kappa) + A_3 x_1(b)x_2(b, \kappa), \quad (4.21)$$

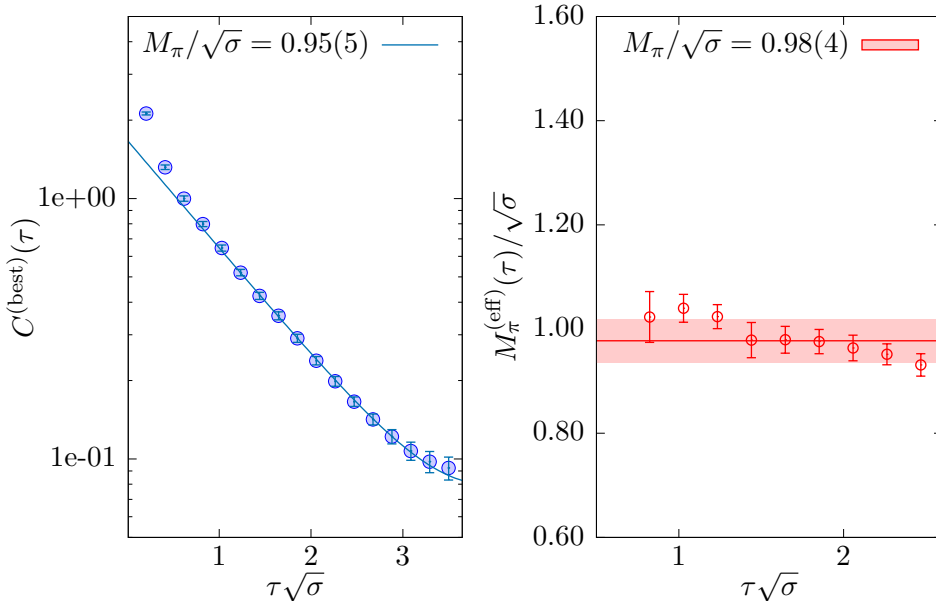


Figure 7: Extraction of the pion mass from the exponential decays of the π optimal correlator obtained from the resolution of the GEVP (left panel). We also show the plateau in the effective masses (right panel). Plots refer to $N = 361$, $b = 0.360$, $\hat{m} = 0.02$, corresponding to $m_\pi\ell = (am_\pi)\sqrt{N} \simeq 3.71$ and $\ell\sqrt{\sigma} = (a\sqrt{\sigma})\sqrt{N} \simeq 3.91$.

where

$$x_1 = a\sqrt{\sigma}, \quad x_2 = \frac{m_\pi^2}{\sigma}, \quad (4.22)$$

and A_1 , A_2 , A_3 are fit parameters. Once A_1 , A_2 and A_3 are determined, the continuum renormalized quark mass as a function of the pion mass is given by the curve:

$$\frac{1}{\sqrt{\sigma}}m_{\text{R}}(m_\pi) = A_2 \frac{m_\pi^2}{\sigma}. \quad (4.23)$$

In Fig. 6 we plot the curve in Eq. (4.23), and on top of it we also show the fitted points ($b = 0.360, 0.365, 0.370, 0.375$) to which we have subtracted lattice artifacts (i.e. the terms proportional to A_1 and A_3). This figure shows the very good quality of the best fit, which has $\tilde{\chi}^2 \simeq 0.84$. On a side note, we observe that $1/(2A_2) = B_{\text{R}}\sqrt{\sigma}$, with $B_{\text{R}}\sqrt{\sigma} = \Sigma_{\text{R}}/(F_\pi^2\sqrt{\sigma})$. We find $B_{\text{R}}/\sqrt{\sigma} = 5.58(22)$, in perfect agreement with the determination $B_{\text{R}}/\sqrt{\sigma} = 5.58(26)$ of [33] from individual b -by- b chiral fits to the quark-mass dependence of the pion mass.

Finally, we measured the overlap pion mass for $\hat{m} = 0.02$, which was found to be:

$$\frac{m_\pi^{(\text{ref})}}{\sqrt{\sigma}} = 0.95(5), \quad (\hat{m} = 0.02 \implies am = 0.0192). \quad (4.24)$$

This will be our reference matching point to compute Z_s from Eq. (4.19), and is reported in Fig. 6 as a solid line. This value is obtained from the customary exponential best fit

to the pion correlator, cf. Fig. 7 (left panel). This correlation function is obtained from a standard GEVP analysis using an extended basis of smeared pseudo-scalar operators. As a standard cross-check, we verified that the effective mass, obtained by solving the GEVP at all times, exhibits a plateau in the same range where we performed the exponential best fit. A constant fit to this plateau gives the perfectly compatible result $\frac{m_{\pi}^{(\text{ref})}}{\sqrt{\sigma}} = 0.98(4)$, cf. Fig. 7 (right panel). For more details on the GEVP analysis we performed, we refer the reader to Ref. [33], a dedicated paper on the extraction of the low-lying meson spectrum of large- N QCD from the TEK model.

The renormalization constant from Eq. (4.19), matched at the overlap pion and quark mass reported in (4.24), reads:

$$\frac{m_{\text{R}}}{\sqrt{\sigma}} \Big|_{m_{\pi}=m_{\pi}^{(\text{ref})}} = 0.0809(32) \quad \Longrightarrow \quad Z_{\text{S}} = \frac{am/(a\sqrt{\sigma})}{m_{\text{R}}/\sqrt{\sigma}} = 1.153(45). \quad (4.25)$$

In order to check the magnitude of possible finite-size effects affecting our pion mass calculation, we also repeated the matching procedure to obtain Z_{S} for a heavier pion. In particular, we chose $\hat{m} = 0.034$ ($am = 0.03264$), and found that it corresponded to $m_{\pi}/\sqrt{\sigma} = 1.244(24)$, i.e., $m_{\pi}\ell \simeq 4.86$ (which is larger than the smallest value of $m_{\pi}\ell$ used with Wilson fermions in Ref. [33]). Adopting this determination as the reference pion mass leads to $m_{\text{R}}/\sqrt{\sigma} = 0.1388(54)$, cf. Fig. 6 (dashed line), and eventually to $Z_{\text{S}} = 1.143(45)$, which is perfectly compatible with the estimate in Eq. (4.25).

Considering our final result for the bare overlap condensate in lattice units obtained in the previous section,

$$\frac{a^3\Sigma}{N} = 0.605(35) \times 10^{-3}, \quad (4.26)$$

and using Z_{S} in Eq. (4.25), we finally find, for the renormalized condensate in physical units:

$$\frac{\Sigma_{\text{R}}}{N\sqrt{\sigma^3}} = 0.0800(63) \quad (b = 0.360, \text{ overlap}). \quad (4.27)$$

It is now interesting to compare our overlap result with the large- N TEK Wilson determination of [33]. On general grounds, overlap fermions are expected to be affected by $\mathcal{O}(a^2)$ leading lattice artifacts, as opposed to Wilson fermions, which instead suffer for $\mathcal{O}(a)$ corrections to the continuum limit. This means that overlap fermions are expected to exhibit a faster convergence towards the continuum limit. This different behavior is due to the fact that they enjoy the lattice chiral symmetry, unlike Wilson fermions. Because of this, overlap and Wilson results obtained at the same value of b do not need to agree. For the same lattice spacing, $b = 0.360$, we found with Wilson fermions in the chiral limit [33]:

$$\frac{\Sigma_{\text{R}}}{N\sqrt{\sigma^3}} = 0.0711(46) \quad (b = 0.360, \text{ Wilson}). \quad (4.28)$$

In the continuum limit, instead:

$$\frac{\Sigma_{\text{R}}}{N\sqrt{\sigma^3}} = 0.0889(23) \quad (\text{continuum limit, Wilson}). \quad (4.29)$$

Our overlap result is indeed much closer to the continuum value with respect to the Wilson one obtained at the same lattice spacing. Our overlap result is thus perfectly consistent with the general theoretical expectation that overlap quarks exhibit a faster convergence towards the continuum limit by virtue of the lattice chiral symmetry.

5 Conclusions

We have presented the first investigation of the universal features of chiral symmetry breaking in large- N QCD from the TEK model, whose employment allowed us to reach N as large as $N = 841$.

Adopting a chiral formulation of the Dirac operator, first presented in this study for the TEK model, we showed clear evidence that the low-lying massless Dirac spectrum of large- N QCD follows RMT predictions when the effective size in physical units $\ell = a\sqrt{N}$ is sufficiently large, both by comparing scale-invariant analytic results with numerical data, and by best fitting lattice eigenvalue probability distributions to RMT functional forms. Chiral condensate determinations extracted from the first few low-lying eigenvalues differ at finite N , but come together as N is increased, confirming that eventually only one single free-parameter describes them all in the thermodynamic limit, as expected from RMT. After renormalization, our overlap determination of the chiral condensate, despite being obtained for a single value of the lattice spacing, turns out to be very close to the continuum TEK determination obtained in [33] from Wilson fermions. This fact is in perfect agreement with the general theoretical expectation that overlap quarks are affected by smaller $\mathcal{O}(a^2)$ lattice artifacts — compared to the $\mathcal{O}(a)$ affecting Wilson quarks — by virtue of the lattice chiral symmetry. Clearly, overlap and Wilson determinations will only fully coincide in the continuum limit.

There are many future research directions that could be explored with overlap fermions. It would be very interesting to extend the present study by investigating the quark-mass behavior of the pion mass, as well as of other mesons, or to study the continuum limit of the chiral condensate. The latter would require an ambitious numerical effort, but also a better theoretical characterization of finite-volume effects in the ϵ -regime of the TEK formulation of large- N QCD. Finally, it would be very interesting to extend the use of the chiral lattice Dirac operator to other large- N gauge theories where chiral symmetry breaking plays a crucial role, such as $\mathcal{N} = 1$ SUSY Yang–Mills, where the calculation of the gluino condensate is of great theoretical interest.

Acknowledgements

It is a pleasure to thank Carlos Pena for many fruitful discussions and for reading this manuscript. We also acknowledge useful discussions with Pilar Hernández and Rajamani Narayanan. This work is partially supported by the Spanish Research Agency (Agencia Estatal de Investigación) through the grant IFT Centro de Excelencia Severo Ochoa CEX2020-001007-S and, partially, by the grant PID2021-127526NB-I00, both funded by

MCIN/AEI/10.13039/ 501100011033. It is also partially funded by the European Commission – NextGenerationEU, through Momentum CSIC Programme: Develop Your Digital Talent. K.-I. I. is supported in part by MEXT as “Feasibility studies for the next-generation computing infrastructure”. This research was supported in part by grant NSF PHY-2309135 to the Kavli Institute for Theoretical Physics (KITP). We acknowledge support from the SFT Scientific Initiative of INFN. This work was partially supported by the Simons Foundation grant 994300 (Simons Collaboration on Confinement and QCD Strings). Numerical calculations have been performed on the *Finisterrae* III cluster at CESGA (Centro de Supercomputación de Galicia), on the *Drago* cluster at CSIC (Consejo Superior de Investigaciones Científicas) and on the Hydra and Ciclope clusters at IFT. We acknowledge HPC support by Emilio Ambite, staff hired under the Generation D initiative, promoted by Red.es, an organization attached to the Ministry for Digital Transformation and the Civil Service, for the attraction and retention of talent through grants and training contracts, financed by the Recovery, Transformation and Resilience Plan through the European Union’s Next Generation funds. We have also used computational resource of Oakbridge-CX, at the University of Tokyo through the HPCI System Research Project (Project ID: hp230021 and hp220011), of Cygnus at Center for Computational Sciences, University of Tsukuba, of SQUID at D3 Center of Osaka university through the RCNP joint use program.

Appendix

A The spectrum of the free overlap operator

In this Appendix we discuss how to restore physical units in the lattice overlap operator D , leading to the rescaling formulas presented in Eqs. (3.25)–(3.29).

Let us start by generically parameterizing the free massless overlap operator in Fourier space by:

$$D_0(p) = \frac{1 + V^{(\text{free})}(p)}{2} = \frac{1}{2} + \frac{B(p) + i \sum_{\mu} \gamma_{\mu} A_{\mu}(p)}{2 \left[B^2(p) + \sum_{\mu} A_{\mu}^2(p) \right]^{1/2}}. \quad (\text{A.1})$$

From this formula one can easily check that the eigenvalues of the operator $H^2 = D_0^{\dagger} D_0$, with $H = \gamma_5 D_0$, are given by:

$$\tilde{\lambda}^2 = \frac{1}{2} + \frac{B(p)}{2 \left[B^2 + \sum_{\mu} A_{\mu}^2(p) \right]^{1/2}}. \quad (\text{A.2})$$

Moreover, making use of the Ginsparg–Wilson relation:

$$D_0 \gamma_5 + \gamma_5 D_0 = 2 D_0 \gamma_5 D_0, \quad (\text{A.3})$$

and the fact that $\gamma_5 D_0 \gamma_5 = D_0^{\dagger}$, one can relate the eigenvalues of D_0 with $\tilde{\lambda}^2$ using that,

$$D_0 + D_0^{\dagger} = 2 H^2, \quad (\text{A.4})$$

therefore $\text{Re}\{\hat{\lambda}\} = \tilde{\lambda}^2$. Making use of the fact that the eigenvalues of D_0 lie on a circle and writing

$$\hat{\lambda} = \frac{1}{2}(1 + e^{i\theta}), \quad (\text{A.5})$$

it is trivial to derive the form of the imaginary part of the eigenvalues, leading to:

$$\hat{\lambda} = \tilde{\lambda}^2 \pm i\tilde{\lambda}\sqrt{1 - \tilde{\lambda}^2}. \quad (\text{A.6})$$

One can now specialize to the case of the overlap operator with kernel given by (3.20). For this, one should first note that the spectrum of the free Wilson–Dirac operator $\gamma_5 D_W(-M)$ in momentum space in the TEK formulation is identical to the standard one, defined on a lattice of $(\sqrt{N})^4$ sites. Using this, one can easily derive the expressions corresponding to $A_\mu(p)$ and $B(p)$ for the overlap kernel used in our work:

$$A_\mu(p) = \frac{2s_\mu}{s^2 + (2 + 2\hat{s}^2 - M)^2}, \quad (\text{A.7})$$

$$B(p) = \frac{s^2 + (2\hat{s}^2 - M)(2 + 2\hat{s}^2 - M)}{s^2 + (2 + 2\hat{s}^2 - M)^2}, \quad (\text{A.8})$$

where $s_\mu = \sin(ap_\mu)$, $s^2 = \sum_\mu \sin^2(ap_\mu)$ and $\hat{s}^2 = \sum_\mu \sin^2(ap_\mu/2)$, with $p_\mu = 2\pi n_\mu/\sqrt{N}$, $n_\mu = 0, \dots, \sqrt{N} - 1$. These results agree with those quoted for the standard overlap operator with identical kernel in Ref. [134].

Once we know the expressions for the eigenvalues, the scaling factor in Eq. (3.29) is obtained by taking into account, for instance, that the eigenvalue corresponding to H^2 in the continuum should be $|p|^2$. The overall scaling factor is easily determined by taking the limit of small ap_μ of $\tilde{\lambda}$, which leads to:

$$\tilde{\lambda}^2 \xrightarrow{a \rightarrow 0} \frac{a^2 |p|^2}{M^2(2 - M)^2}, \quad (\text{A.9})$$

i.e., the factor of $M(2 - M)/a$ appearing in Eqs. (3.25)–(3.29).

References

- [1] T. Banks and A. Casher, *Chiral Symmetry Breaking in Confining Theories*, *Nucl. Phys. B* **169** (1980) 103.
- [2] H. Leutwyler and A. V. Smilga, *Spectrum of Dirac operator and role of winding number in QCD*, *Phys. Rev. D* **46** (1992) 5607.
- [3] E. V. Shuryak and J. J. M. Verbaarschot, *Random matrix theory and spectral sum rules for the Dirac operator in QCD*, *Nucl. Phys. A* **560** (1993) 306 [[hep-th/9212088](#)].
- [4] J. J. M. Verbaarschot and I. Zahed, *Spectral density of the QCD Dirac operator near zero virtuality*, *Phys. Rev. Lett.* **70** (1993) 3852 [[hep-th/9303012](#)].
- [5] J. J. M. Verbaarschot, *The Spectrum of the QCD Dirac operator and chiral random matrix theory: The Threefold way*, *Phys. Rev. Lett.* **72** (1994) 2531 [[hep-th/9401059](#)].

- [6] S. M. Nishigaki, P. H. Damgaard and T. Wettig, *Smallest Dirac eigenvalue distribution from random matrix theory*, *Phys. Rev. D* **58** (1998) 087704 [[hep-th/9803007](#)].
- [7] R. G. Edwards, U. M. Heller, J. E. Kiskis and R. Narayanan, *Quark spectra, topology and random matrix theory*, *Phys. Rev. Lett.* **82** (1999) 4188 [[hep-th/9902117](#)].
- [8] P. H. Damgaard, R. G. Edwards, U. M. Heller and R. Narayanan, *Universal scaling of the chiral condensate in finite volume gauge theories*, *Phys. Rev. D* **61** (2000) 094503 [[hep-lat/9907016](#)].
- [9] W. Bietenholz, K. Jansen and S. Shcheredin, *Spectral properties of the overlap Dirac operator in QCD*, *JHEP* **07** (2003) 033 [[hep-lat/0306022](#)].
- [10] L. Giusti, M. Luscher, P. Weisz and H. Wittig, *Lattice QCD in the epsilon regime and random matrix theory*, *JHEP* **11** (2003) 023 [[hep-lat/0309189](#)].
- [11] J. Wennekers and H. Wittig, *On the renormalized scalar density in quenched QCD*, *JHEP* **09** (2005) 059 [[hep-lat/0507026](#)].
- [12] F. Bernardoni, P. H. Damgaard, H. Fukaya and P. Hernandez, *Finite Volume Scaling of Pseudo Nambu-Goldstone Bosons in QCD*, *JHEP* **10** (2008) 008 [[0808.1986](#)].
- [13] A. Hasenfratz, R. Hoffmann and S. Schaefer, *Low energy chiral constants from epsilon-regime simulations with improved Wilson fermions*, *Phys. Rev. D* **78** (2008) 054511 [[0806.4586](#)].
- [14] F. Bernardoni, P. Hernandez, N. Garron, S. Necco and C. Pena, *Probing the chiral regime of $N_f = 2$ QCD with mixed actions*, *Phys. Rev. D* **83** (2011) 054503 [[1008.1870](#)].
- [15] A. Deuzeman, U. Wenger and J. Wuilloud, *Spectral properties of the Wilson Dirac operator in the ϵ -regime*, *JHEP* **12** (2011) 109 [[1110.4002](#)].
- [16] M. Catillo and L. Y. Glozman, *Distribution law of the Dirac eigenmodes in QCD*, *Int. J. Mod. Phys. A* **33** (2018) 1850054 [[1709.01886](#)].
- [17] T. G. Kovacs and F. Pittler, *Poisson to Random Matrix Transition in the QCD Dirac Spectrum*, *Phys. Rev. D* **86** (2012) 114515 [[1208.3475](#)].
- [18] M. Giordano, T. G. Kovacs and F. Pittler, *Universality and the QCD Anderson Transition*, *Phys. Rev. Lett.* **112** (2014) 102002 [[1312.1179](#)].
- [19] T. G. Kovacs and R. A. Vig, *Localization transition in $SU(3)$ gauge theory*, *Phys. Rev. D* **97** (2018) 014502 [[1706.03562](#)].
- [20] R. A. Vig and T. G. Kovacs, *Localization with overlap fermions*, *Phys. Rev. D* **101** (2020) 094511 [[2001.06872](#)].
- [21] M. Giordano and T. G. Kovacs, *Localization of Dirac Fermions in Finite-Temperature Gauge Theory*, *Universe* **7** (2021) 194 [[2104.14388](#)].
- [22] J. J. M. Verbaarschot and T. Wettig, *Random matrix theory and chiral symmetry in QCD*, *Ann. Rev. Nucl. Part. Sci.* **50** (2000) 343 [[hep-ph/0003017](#)].
- [23] P. H. Damgaard, *The Microscopic Dirac operator spectrum*, *Nucl. Phys. B Proc. Suppl.* **106** (2002) 29 [[hep-lat/0110192](#)].
- [24] J. J. M. Verbaarschot, *Handbook Article on Applications of Random Matrix Theory to QCD*, [0910.4134](#).

- [25] P. H. Damgaard, *Chiral Random Matrix Theory and Chiral Perturbation Theory*, *J. Phys. Conf. Ser.* **287** (2011) 012004 [[1102.1295](#)].
- [26] R. Narayanan and H. Neuberger, *The Quark mass dependence of the pion mass at infinite N* , *Phys. Lett. B* **616** (2005) 76 [[hep-lat/0503033](#)].
- [27] L. Del Debbio, B. Lucini, A. Patella and C. Pica, *Quenched mesonic spectrum at large N* , *JHEP* **03** (2008) 062 [[0712.3036](#)].
- [28] G. S. Bali, F. Bursa, L. Castagnini, S. Collins, L. Del Debbio, B. Lucini et al., *Mesons in large- N QCD*, *JHEP* **06** (2013) 071 [[1304.4437](#)].
- [29] T. DeGrand and Y. Liu, *Lattice study of large N_c QCD*, *Phys. Rev. D* **94** (2016) 034506 [[1606.01277](#)].
- [30] P. Hernández, C. Pena and F. Romero-López, *Large N_c scaling of meson masses and decay constants*, *Eur. Phys. J. C* **79** (2019) 865 [[1907.11511](#)].
- [31] T. A. DeGrand and E. Wickenden, *Lattice study of the chiral properties of large N_c QCD*, [2309.12270](#).
- [32] C. Bonanno, P. Butti, M. García Pérez, A. González-Arroyo, K.-I. Ishikawa and M. Okawa, *The large- N limit of the chiral condensate from twisted reduced models*, *JHEP* **12** (2023) 034 [[2309.15540](#)].
- [33] C. Bonanno, M. García Pérez, A. González-Arroyo, K.-I. Ishikawa and M. Okawa, *Non-perturbative determination of meson masses and low-energy constants in large- N QCD*, [2508.05446](#).
- [34] R. Narayanan and H. Neuberger, *Chiral symmetry breaking at large N_c* , *Nucl. Phys. B* **696** (2004) 107 [[hep-lat/0405025](#)].
- [35] A. González-Arroyo, R. Narayanan and H. Neuberger, *Large N reduction on a twisted torus*, *Phys. Lett. B* **631** (2005) 133 [[hep-lat/0509074](#)].
- [36] M. Hanada, J.-W. Lee and N. Yamada, *Large- N_c gauge theory and chiral random matrix theory*, *Phys. Rev. D* **88** (2013) 025046 [[1302.3532](#)].
- [37] A. González-Arroyo and M. Okawa, *A twisted model for large- N lattice gauge theory*, *Physics Letters B* **120** (1983) 174.
- [38] A. González-Arroyo and M. Okawa, *Twisted-eguchi-kawai model: A reduced model for large- N lattice gauge theory*, *Phys. Rev. D* **27** (1983) 2397.
- [39] A. González-Arroyo and M. Okawa, *Large N reduction with the Twisted Eguchi-Kawai model*, *JHEP* **07** (2010) 043 [[1005.1981](#)].
- [40] T. Eguchi and H. Kawai, *Reduction of dynamical degrees of freedom in the large- N gauge theory*, *Phys. Rev. Lett.* **48** (1982) 1063.
- [41] G. Bhanot, U. M. Heller and H. Neuberger, *The quenched Eguchi-Kawai model*, *Physics Letters B* **113** (1982) 47.
- [42] D. J. Gross and Y. Kitazawa, *A Quenched Momentum Prescription for Large N Theories*, *Nucl. Phys. B* **206** (1982) 440.
- [43] G. Aldazabal, N. Parga, M. Okawa and A. González-Arroyo, *Large N Reduced Models and Stochastic Quantization*, *Phys. Lett. B* **129** (1983) 90.

- [44] J. Kiskis, R. Narayanan and H. Neuberger, *Proposal for the numerical solution of planar QCD*, *Phys. Rev. D* **66** (2002) 025019 [[hep-lat/0203005](#)].
- [45] R. Narayanan and H. Neuberger, *Large N reduction in continuum*, *Phys. Rev. Lett.* **91** (2003) 081601 [[hep-lat/0303023](#)].
- [46] P. Kovtun, M. Unsal and L. G. Yaffe, *Volume independence in large $N(c)$ QCD-like gauge theories*, *JHEP* **06** (2007) 019 [[hep-th/0702021](#)].
- [47] M. Unsal and L. G. Yaffe, *Center-stabilized Yang-Mills theory: Confinement and large N volume independence*, *Phys. Rev. D* **78** (2008) 065035 [[0803.0344](#)].
- [48] H. Neuberger, *Quenched Eguchi-Kawai model revisited*, *Phys. Rev. D* **102** (2020) 094503 [[2009.09539](#)].
- [49] A. González-Arroyo and M. Okawa, *String Tension for Large N Gauge Theory*, *Phys. Lett. B* **133** (1983) 415.
- [50] S. R. Das and J. B. Kogut, *On the Deconfining Transition of $SU(\text{Infinity})$ Gauge Theory*, *Nucl. Phys. B* **257** (1985) 141.
- [51] S. R. Das and J. B. Kogut, *Evidence for a First Order Deconfinement Transition in Large N Gauge Theory*, *Phys. Rev. D* **31** (1985) 2704.
- [52] J. Kiskis and R. Narayanan, *Computation of the string tension in four-dimensional Yang-Mills theory using large N reduction*, *Phys. Lett. B* **681** (2009) 372 [[0908.1451](#)].
- [53] A. Hietanen and R. Narayanan, *The large N limit of four dimensional Yang-Mills field coupled to adjoint fermions on a single site lattice*, *JHEP* **01** (2010) 079 [[0911.2449](#)].
- [54] A. Hietanen and R. Narayanan, *Large- N reduction of $SU(N)$ Yang-Mills theory with massive adjoint overlap fermions*, *Phys. Lett. B* **698** (2011) 171 [[1011.2150](#)].
- [55] B. Bringoltz, M. Koren and S. R. Sharpe, *Large- N reduction in QCD with two adjoint Dirac fermions*, *Phys. Rev. D* **85** (2012) 094504 [[1106.5538](#)].
- [56] A. Hietanen and R. Narayanan, *Numerical evidence for non-analytic behavior in the beta function of large N $SU(N)$ gauge theory coupled to an adjoint Dirac fermion*, *Phys. Rev. D* **86** (2012) 085002 [[1204.0331](#)].
- [57] A. González-Arroyo and M. Okawa, *The string tension from smeared Wilson loops at large N* , *Phys. Lett. B* **718** (2013) 1524 [[1206.0049](#)].
- [58] A. González-Arroyo and M. Okawa, *Twisted space-time reduced model of large N QCD with two adjoint Wilson fermions*, *Phys. Rev. D* **88** (2013) 014514 [[1305.6253](#)].
- [59] R. Lohmayer and R. Narayanan, *Weak-coupling analysis of the single-site large- N gauge theory coupled to adjoint fermions*, *Phys. Rev. D* **87** (2013) 125024 [[1305.1279](#)].
- [60] A. González-Arroyo and M. Okawa, *Testing volume independence of $SU(N)$ pure gauge theories at large N* , *JHEP* **12** (2014) 106 [[1410.6405](#)].
- [61] M. García Pérez, A. González-Arroyo, L. Keegan and M. Okawa, *The $SU(\infty)$ twisted gradient flow running coupling*, *JHEP* **01** (2015) 038 [[1412.0941](#)].
- [62] M. García Pérez, A. González-Arroyo, L. Keegan and M. Okawa, *Mass anomalous dimension of Adjoint QCD at large N from twisted volume reduction*, *JHEP* **08** (2015) 034 [[1506.06536](#)].

- [63] M. García Pérez, A. González-Arroyo, L. Keegan, M. Okawa and A. Ramos, *A comparison of updating algorithms for large N reduced models*, *JHEP* **06** (2015) 193 [[1505.05784](#)].
- [64] A. González-Arroyo and M. Okawa, *Large N meson masses from a matrix model*, *Phys. Lett. B* **755** (2016) 132 [[1510.05428](#)].
- [65] M. García Pérez, A. González-Arroyo and M. Okawa, *Perturbative contributions to Wilson loops in twisted lattice boxes and reduced models*, *JHEP* **10** (2017) 150 [[1708.00841](#)].
- [66] M. García Pérez, *Prospects for large N gauge theories on the lattice*, *PoS LATTICE2019* (2020) 276 [[2001.10859](#)].
- [67] M. García Pérez, A. González-Arroyo and M. Okawa, *Meson spectrum in the large N limit*, *JHEP* **04** (2021) 230 [[2011.13061](#)].
- [68] P. Butti and A. González-Arroyo, *Testing (asymptotic) scaling in Yang-Mills theories in the large- N_c limit*, *PoS LATTICE2023* (2024) 381 [[2311.18696](#)].
- [69] P. Butti, M. García Pérez, A. González-Arroyo, K.-I. Ishikawa and M. Okawa, *Scale setting for large- N SUSY Yang-Mills on the lattice*, *JHEP* **07** (2022) 074 [[2205.03166](#)].
- [70] C. Bonanno, P. Butti, M. García Pérez, A. González-Arroyo, K.-I. Ishikawa and M. Okawa, *Nonperturbative determination of the $\mathcal{N} = 1$ supersymmetric Yang-Mills gluino condensate at large N* , *Phys. Rev. D* **110** (2024) 074507 [[2406.08995](#)].
- [71] C. Bonanno, M. García Pérez, A. González-Arroyo, K.-I. Ishikawa and M. Okawa, *The mass of the gluino-gluon bound state in large- N $\mathcal{N} = 1$ Supersymmetric Yang-Mills theory*, *JHEP* **03** (2025) 174 [[2412.02348](#)].
- [72] L. Del Debbio, H. Panagopoulos, P. Rossi and E. Vicari, *Spectrum of confining strings in $SU(N)$ gauge theories*, *JHEP* **01** (2002) 009 [[hep-th/0111090](#)].
- [73] B. Lucini and M. Teper, *$SU(N)$ gauge theories in four-dimensions: Exploring the approach to $N = \infty$* , *JHEP* **06** (2001) 050 [[hep-lat/0103027](#)].
- [74] L. Del Debbio, H. Panagopoulos and E. Vicari, *θ dependence of $SU(N)$ gauge theories*, *JHEP* **08** (2002) 044 [[hep-th/0204125](#)].
- [75] B. Lucini, M. Teper and U. Wenger, *Glueballs and k -strings in $SU(N)$ gauge theories: Calculations with improved operators*, *JHEP* **06** (2004) 012 [[hep-lat/0404008](#)].
- [76] L. Del Debbio, G. M. Manca, H. Panagopoulos, A. Skouroupathis and E. Vicari, *θ -dependence of the spectrum of $SU(N)$ gauge theories*, *JHEP* **06** (2006) 005 [[hep-th/0603041](#)].
- [77] E. Vicari and H. Panagopoulos, *θ dependence of $SU(N)$ gauge theories in the presence of a topological term*, *Phys. Rept.* **470** (2009) 93 [[0803.1593](#)].
- [78] C. Allton, M. Teper and A. Trivini, *On the running of the bare coupling in $SU(N)$ lattice gauge theories*, *JHEP* **07** (2008) 021 [[0803.1092](#)].
- [79] B. Lucini, A. Rago and E. Rinaldi, *Glueball masses in the large- N limit*, *JHEP* **08** (2010) 119 [[1007.3879](#)].
- [80] B. Lucini and M. Panero, *$SU(N)$ gauge theories at large N* , *Phys. Rept.* **526** (2013) 93 [[1210.4997](#)].
- [81] C. Bonati, M. D’Elia, P. Rossi and E. Vicari, *θ dependence of 4D $SU(N)$ gauge theories in the large- N limit*, *Phys. Rev. D* **94** (2016) 085017 [[1607.06360](#)].

- [82] M. Cè, M. García Vera, L. Giusti and S. Schaefer, *The topological susceptibility in the large- N limit of $SU(N)$ Yang-Mills theory*, *Phys. Lett. B* **762** (2016) 232 [[1607.05939](#)].
- [83] E. Bennett, J. Holligan, D. K. Hong, J.-W. Lee, C. J. D. Lin, B. Lucini et al., *Color dependence of tensor and scalar glueball masses in Yang-Mills theories*, *Phys. Rev. D* **102** (2020) 011501 [[2004.11063](#)].
- [84] C. Bonanno, C. Bonati and M. D’Elia, *Large- N $SU(N)$ Yang-Mills theories with milder topological freezing*, *JHEP* **03** (2021) 111 [[2012.14000](#)].
- [85] A. Athenodorou and M. Teper, *$SU(N)$ gauge theories in 3+1 dimensions: glueball spectrum, string tensions and topology*, *JHEP* **12** (2021) 082 [[2106.00364](#)].
- [86] E. Bennett, D. K. Hong, J.-W. Lee, C. J. D. Lin, B. Lucini, M. Piai et al., *Color dependence of the topological susceptibility in Yang-Mills theories*, *Phys. Lett. B* **835** (2022) 137504 [[2205.09254](#)].
- [87] C. Bonanno, M. D’Elia, B. Lucini and D. VDACCHINO, *Towards glueball masses of large- N $SU(N)$ pure-gauge theories without topological freezing*, *Phys. Lett. B* **833** (2022) 137281 [[2205.06190](#)].
- [88] C. Bonanno, C. Bonati, M. Papace and D. VDACCHINO, *The θ -dependence of the Yang-Mills spectrum from analytic continuation*, *JHEP* **05** (2024) 163 [[2402.03096](#)].
- [89] A. Athenodorou, S. Dubovsky, C. Luo and M. Teper, *Confining Strings and the Worldsheet Axion from the Lattice*, [2411.03435](#).
- [90] A. Sharifian, A. Athenodorou and P. Bicudo, *The spectrum of open confining strings in the large- N_c limit*, [2506.16342](#).
- [91] T. DeGrand, *Topological susceptibility in QCD with two flavors and 3-5 colors: a pilot study*, *Phys. Rev. D* **101** (2020) 114509 [[2004.09649](#)].
- [92] P. Hernández and F. Romero-López, *The large N_c limit of QCD on the lattice*, *Eur. Phys. J. A* **57** (2021) 52 [[2012.03331](#)].
- [93] T. DeGrand, *Finite temperature properties of QCD with two flavors and three, four and five colors*, *Phys. Rev. D* **103** (2021) 094513 [[2102.01150](#)].
- [94] J. Baeza-Ballesteros, P. Hernández and F. Romero-López, *A lattice study of $\pi\pi$ scattering at large N_c* , *JHEP* **06** (2022) 049 [[2202.02291](#)].
- [95] T. DeGrand, *Curve collapse for the isospin-2 pion scattering length from QCD with 3, 4, and 5 colors*, [2409.02242](#).
- [96] T. DeGrand, *Comparison of a pseudoscalar meson form factor in QCD with 3, 4, and 5 colors*, [2412.14143](#).
- [97] J. Baeza-Ballesteros, P. Hernández and F. Romero-López, *The $\pi\pi$ scattering amplitude at large N_c* , [2503.13978](#).
- [98] P. Butti, M. Della Morte, B. Jäger, S. Martins and J. T. Tsang, *Comparison of smoothening flows for the topological charge in QCD-like theories*, *Phys. Rev. D* **112** (2025) 014504 [[2504.10197](#)].
- [99] J. Fingberg, U. M. Heller and F. Karsch, *Scaling and asymptotic scaling in the $SU(2)$ gauge theory*, *Nucl. Phys. B* **392** (1993) 493 [[hep-lat/9208012](#)].

- [100] B. Beinlich, F. Karsch, E. Laermann and A. Peikert, *String tension and thermodynamics with tree level and tadpole improved actions*, *Eur. Phys. J. C* **6** (1999) 133 [[hep-lat/9707023](#)].
- [101] M. Campostrini, *The large N phase transition of lattice $SU(N)$ gauge theories*, *Nucl. Phys. B Proc. Suppl.* **73** (1999) 724 [[hep-lat/9809072](#)].
- [102] B. Lucini, M. Teper and U. Wenger, *The Deconfinement transition in $SU(N)$ gauge theories*, *Phys. Lett. B* **545** (2002) 197 [[hep-lat/0206029](#)].
- [103] B. Lucini, M. Teper and U. Wenger, *The High temperature phase transition in $SU(N)$ gauge theories*, *JHEP* **01** (2004) 061 [[hep-lat/0307017](#)].
- [104] B. Lucini, M. Teper and U. Wenger, *Topology of $SU(N)$ gauge theories at $T \simeq 0$ and $T \simeq T_c$* , *Nucl. Phys. B* **715** (2005) 461 [[hep-lat/0401028](#)].
- [105] B. Lucini, M. Teper and U. Wenger, *Properties of the deconfining phase transition in $SU(N)$ gauge theories*, *JHEP* **02** (2005) 033 [[hep-lat/0502003](#)].
- [106] B. Lucini, A. Rago and E. Rinaldi, *$SU(N_c)$ gauge theories at deconfinement*, *Phys. Lett. B* **712** (2012) 279 [[1202.6684](#)].
- [107] S. Borsanyi, K. R., Z. Fodor, D. A. Godzieba, P. Parotto and D. Sexty, *Precision study of the continuum $SU(3)$ Yang-Mills theory: How to use parallel tempering to improve on supercritical slowing down for first order phase transitions*, *Phys. Rev. D* **105** (2022) 074513 [[2202.05234](#)].
- [108] B. Lucini, D. Mason, M. Piai, E. Rinaldi and D. Vadacchino, *First-order phase transitions in Yang-Mills theories and the density of state method*, [2305.07463](#).
- [109] T. D. Cohen and L. Y. Glozman, *Large N_c QCD phase diagram at $\mu_B = 0$* , *Eur. Phys. J. A* **60** (2024) 171 [[2311.07333](#)].
- [110] Y. Hamada and T. Misumi, *\mathbb{Z}_N stability and continuity in twisted Eguchi-Kawai model with two-flavor adjoint fermions*, [2507.20123](#).
- [111] P. H. Ginsparg and K. G. Wilson, *A Remnant of Chiral Symmetry on the Lattice*, *Phys. Rev. D* **25** (1982) 2649.
- [112] H. Neuberger, *Exactly massless quarks on the lattice*, *Phys. Lett. B* **417** (1998) 141 [[hep-lat/9707022](#)].
- [113] H. Neuberger, *More about exactly massless quarks on the lattice*, *Phys. Lett. B* **427** (1998) 353 [[hep-lat/9801031](#)].
- [114] M. Lüscher, *Exact chiral symmetry on the lattice and the Ginsparg-Wilson relation*, *Phys. Lett. B* **428** (1998) 342 [[hep-lat/9802011](#)].
- [115] D. B. Kaplan, *A Method for simulating chiral fermions on the lattice*, *Phys. Lett. B* **288** (1992) 342 [[hep-lat/9206013](#)].
- [116] Y. Shamir, *Chiral fermions from lattice boundaries*, *Nucl. Phys. B* **406** (1993) 90 [[hep-lat/9303005](#)].
- [117] V. Furman and Y. Shamir, *Axial symmetries in lattice QCD with Kaplan fermions*, *Nucl. Phys. B* **439** (1995) 54 [[hep-lat/9405004](#)].
- [118] A. Borici, *Truncated overlap fermions*, *Nucl. Phys. B Proc. Suppl.* **83** (2000) 771 [[hep-lat/9909057](#)].

- [119] R. G. Edwards and U. M. Heller, *Domain wall fermions with exact chiral symmetry*, *Phys. Rev. D* **63** (2001) 094505 [[hep-lat/0005002](#)].
- [120] K.-I. Ishikawa, *Testing reweighting method for truncated Overlap fermions*, [1310.8022](#).
- [121] P. H. Damgaard and S. M. Nishigaki, *Distribution of the k -th smallest Dirac operator eigenvalue*, *Phys. Rev. D* **63** (2001) 045012 [[hep-th/0006111](#)].
- [122] F. Chamizo and A. González-Arroyo, *Tachyonic instabilities in 2 + 1 dimensional Yang–Mills theory and its connection to number theory*, *J. Phys. A* **50** (2017) 265401 [[1610.07972](#)].
- [123] M. García Pérez, A. González-Arroyo, M. Koren and M. Okawa, *The spectrum of 2+1 dimensional Yang–Mills theory on a twisted spatial torus*, *JHEP* **07** (2018) 169 [[1807.03481](#)].
- [124] T. Ishikawa and M. Okawa, *Z_N^D symmetry breaking on the numerical simulation of twisted Eguchi–Kawai model, talk given at the Annual Meeting of the Physical Society of Japan, March 28–31, Sendai, Japan (2003)*.
- [125] W. Bietenholz, J. Nishimura, Y. Susaki and J. Volkholz, *A Non-perturbative study of 4-D $U(1)$ non-commutative gauge theory: The Fate of one-loop instability*, *JHEP* **10** (2006) 042 [[hep-th/0608072](#)].
- [126] M. Teper and H. Vairinhos, *Symmetry breaking in twisted Eguchi–Kawai models*, *Phys. Lett. B* **652** (2007) 359 [[hep-th/0612097](#)].
- [127] T. Azeyanagi, M. Hanada, T. Hirata and T. Ishikawa, *Phase structure of twisted Eguchi–Kawai model*, *JHEP* **01** (2008) 025 [[0711.1925](#)].
- [128] E. I. Bribián and M. García Pérez, *The twisted gradient flow coupling at one loop*, *JHEP* **03** (2019) 200 [[1903.08029](#)].
- [129] A. González-Arroyo, *Yang–Mills fields on the four-dimensional torus. Part 1.: Classical theory*, in *Advanced Summer School on Nonperturbative Quantum Field Physics*, pp. 57–91, 6, 1997, [[hep-th/9807108](#)].
- [130] Y. Kikukawa and T. Noguchi, *Low-energy effective action of domain wall fermion and the Ginsparg–Wilson relation*, *Nucl. Phys. B Proc. Suppl.* **83** (2000) 630 [[hep-lat/9902022](#)].
- [131] R. C. Brower, H. Neff and K. Orginos, *Mobius fermions*, *Nucl. Phys. B Proc. Suppl.* **153** (2006) 191 [[hep-lat/0511031](#)].
- [132] C. Morningstar and M. J. Peardon, *Analytic smearing of $SU(3)$ link variables in lattice QCD*, *Phys. Rev. D* **69** (2004) 054501 [[hep-lat/0311018](#)].
- [133] T.-W. Chiu, *Optimal domain wall fermions*, *Phys. Rev. Lett.* **90** (2003) 071601 [[hep-lat/0209153](#)].
- [134] S. Aoki and Y. Taniguchi, *Chiral properties of domain wall fermions from eigenvalues of four-dimensional Wilson–Dirac operator*, *Phys. Rev. D* **65** (2002) 074502 [[hep-lat/0109022](#)].
- [135] L. Del Debbio, L. Giusti and C. Pica, *Topological susceptibility in the $SU(3)$ gauge theory*, *Phys. Rev. Lett.* **94** (2005) 032003 [[hep-th/0407052](#)].
- [136] C. Alexandrou, A. Athenodorou, K. Cichy, A. Dromard, E. García-Ramos, K. Jansen et al., *Comparison of topological charge definitions in Lattice QCD*, *Eur. Phys. J. C* **80** (2020) 424 [[1708.00696](#)].

- [137] S. Borsanyi et al., *Leading hadronic contribution to the muon magnetic moment from lattice QCD*, *Nature* **593** (2021) 51 [[2002.12347](#)].
- [138] A. Boccaletti et al., *High precision calculation of the hadronic vacuum polarisation contribution to the muon anomaly*, [2407.10913](#).
- [139] J. Gasser and H. Leutwyler, *Thermodynamics of Chiral Symmetry*, *Phys. Lett. B* **188** (1987) 477.
- [140] F. Basile and G. Akemann, *Equivalence of QCD in the epsilon-regime and chiral random matrix theory with or without chemical potential*, *JHEP* **12** (2007) 043 [[0710.0376](#)].
- [141] L. Castagnini, *Meson spectroscopy in Large- N QCD*, [[inspirehep/1411974](#)] (2015) .